PROCEEDINGS, 50th Workshop on Geothermal Reservoir Engineering
Stanford University, Stanford, California, February 10-12, 2025
SGP-TR-229

Geochemical Evaluation of Scale Types in a Production Well Following the 2018 Kilauea Eruption, Puna Geothermal Venture, Hawaii, USA

Derek Caro, Adam Johnson, Ed Mroczek, Nick Prina, Drew Spake, Joseph Heimerl, Scott Costa, Paul Spielman

Ormat Technologies, 6884 Sierra Center Parkway, Reno, NV 89511

dcaro@ormat.com

Keywords: Puna Geothermal Venture, geochemistry, scale, seawater, basalt, XRD, XRF

ABSTRACT

The Puna geothermal field commenced production in 1993 and is presently operated by the Puna Geothermal Venture (PGV), which was acquired by Ormat Technologies (Ormat) in 2004. The geothermal field is hosted in basalt and discharges a diluted hydrothermally altered seawater. An eruption occurred in 2018 in the Lower East Rift Zone (LERZ) which resulted in the temporary shut in of all wells. Due to damage caused by the eruption, some wells have been abandoned, whilst some have had mechanical repairs and redrills conducted. KS-14 was a production well that was in operation prior to the 2018 eruption. Following the eruption, the well was mechanically repaired with the installation of an additional production liner. The original reservoir section was abandoned, and another reservoir section was drilled to a new bottom hole target, as KS-14RD2. The well was then put in service but ceased to flow in mid-2023. A mechanical cleanout was undertaken and a total of 14 solid debris samples were collected originating from depths ranging between 1,879 ft and 5,255 ft. These samples have been geochemically characterized and this paper highlights the results of these analyses and discusses the context of these scale types.

1. INTRODUCTION

The Puna Geothermal Field is a high temperature (~325°C) two-phase liquid dominated system located in the Lower East Rift Zone (LERZ) of the Kilauea volcano on the island of Hawai'i. An updated conceptual model of the field based on extensive geoscientific data collected since the 1960's was recently presented by Spake et al. (2024). This included a summary of the production history, which commenced commercial operation in 1993. Presently, the power station includes nine of the original air-cooled Ormat combined cycle units (steam turbine with binary condenser) and two air-cooled brine binary units with a total nominal capacity of 38 MW net. All production wells at PGV exhibit artesian conditions, with production of two-phase brine and steam or single-phase steam. Since the beginning of commercial operation in 1993, the plant has operated with 100% reinjection of geothermal brine, steam condensate, and non-condensable gases (NCG's) resulting in zero emissions from the geothermal reservoir.

Due to high permeability of the regional basalts, cold seawater infiltrates deep into the LERZ and fully equilibrates with basalt at the elevated temperature and is further diluted with altered meteoric water, resulting in a variably mixed geothermal seawater system with a total dissolved solids (TDS) content of between 1-2 weight percent, representing roughly 40 to 80% seawater contribution. The interaction between seawater and basalt rock at elevated temperatures leads to significant geochemical transformations of the seawater, including the alteration of major reactive constituents (e.g., Na, K, Mg, SO4). The basalts of the LERZ are also high in iron as titanium-bearing magnetite, ferrian ilmenite, olivine (Anderson and Wright, 1972; Gerlach, 1993) and other trace metals which are released by the reaction of the basalt with seawater and transported as metal sulfide and chloride complexes.

The most significant and disruptive event in the history of the Puna geothermal field was the 2018 Kilauea eruption within the LERZ, which forced the closure of the power station and shut in of all wells until the eruption subsided. Murphy et al., 2024 outlined the temperature, permeability, and pressure response of the geothermal resource during the eruption and following plant startup. Those results showed that permeability distribution changed as some well-known fractures lost permeability, while others remained permeable. In addition, reservoir temperatures and pressures recovered to near pre-operational conditions as a result of significant heat input to the geothermal system. In conjunction with these impacts on the reservoir, geochemical changes consistent with a change in the proportion of thermally altered seawater to meteoric water as well as an increase in gas abundance were observed. Continued geochemical monitoring has shown that the geochemical signature of the reservoir has been dynamic, transitioning back to near pre-eruption conditions over the last several years. As a result, geochemical characteristics immediately following the eruption likely do not reflect historic and/or future conditions.

Post-eruption, the resulting damage led to the abandonment of several wells and the need for mechanical workovers and redrills of others. Repaired wells included the historic KS-14, which was repaired with a cemented scab liner, and redrilled to a new bottomhole target as KS-14RD2 (referred to as KS-14 hereinafter) with a downhole maximum static temperature of 332°C. The well was put back into production in early-2021, but ceased to flow in mid-2023, inferred to be due to wellbore scaling. In early-2024 there was an attempt to mechanically workover the well to remove scale. The mechanical cleaning was ultimately unsuccessful in recovering the well, which has been idle since the workover attempt and is being considered for conversion to a pressure monitoring well. Despite being unable to bring KS-14 back into production, 14 solid debris samples were collected at a variety of depths during the cleanout attempt. These samples

were submitted to laboratories for mineralogical and elemental analysis to provide context on the type of scales resulting from production and improve understanding of how these materials may have played a role in the failure of the well.

2. BACKGROUND INFORMATION

2.2 KS-14 Well Construction and Design

Following the 2018 eruption, drilling rig operations to bring KS-14 back into service were initiated in July of 2019. After drilling out the heavy mud plug placed during the eruption to control pressure and plug the wellbore, the hole was washed and reamed to a depth of 4,730 feet (Spielman, et al., 2020). A caliper log was run and showed severe casing damage at 2,100 ft and from 2,186 to 2,210 ft. The log data was poor beneath these depths, but drilling data indicated additional damage zones likely existed below 2,200 ft. Several cement plugs were set at a variety of depths throughout the wellbore to stabilize the hole and prepare it for installation of a scab liner. Heavy wall 8-5/8" casing (scab liner) was run and cemented inside the 11-3/4" production casing from 1,879 ft to 4,609 ft (Figure 1) to cover damage zones and ensure integrity of the production string. Mechanical cleaning operations continued through the shoe of the scab liner and encountered a tight spot, with formation returns, suggesting an unintentional sidetrack had occurred around 4,635'. The side-track was confirmed with directional data and Redrill No.1 (KS-14RD1) was initiated. KS-14RD1 was drilled with a conventional BHA and a 6-3/4" bit to 5,364 ft, with full circulation. Due to the lack of commercial permeability, cement was pumped to plug and abandon Redrill No. 1. Redrill No. 2 (KS-14RD2) was directionally drilled to 5,565 ft where the directional tools were pulled and replaced with a slick BHA and a 6-3/4" bit to drill into the production zone. The KS-14 production fracture was crossed at 5,580 ft with full circulation, indicating potential eruption-related sealing of the fracture at this depth. Drilling continued to 5,727 ft (total depth) with numerous drilling breaks and mud losses starting at 5,614 ft. A 5" slotted liner was run and set on bottom at 5,727 ft with top at 4,592 ft. The slotted section of the 5" liner ran from roughly 5,482 ft to 5,727 ft and targets the current production zone. The general well design is shown in Figure 1.

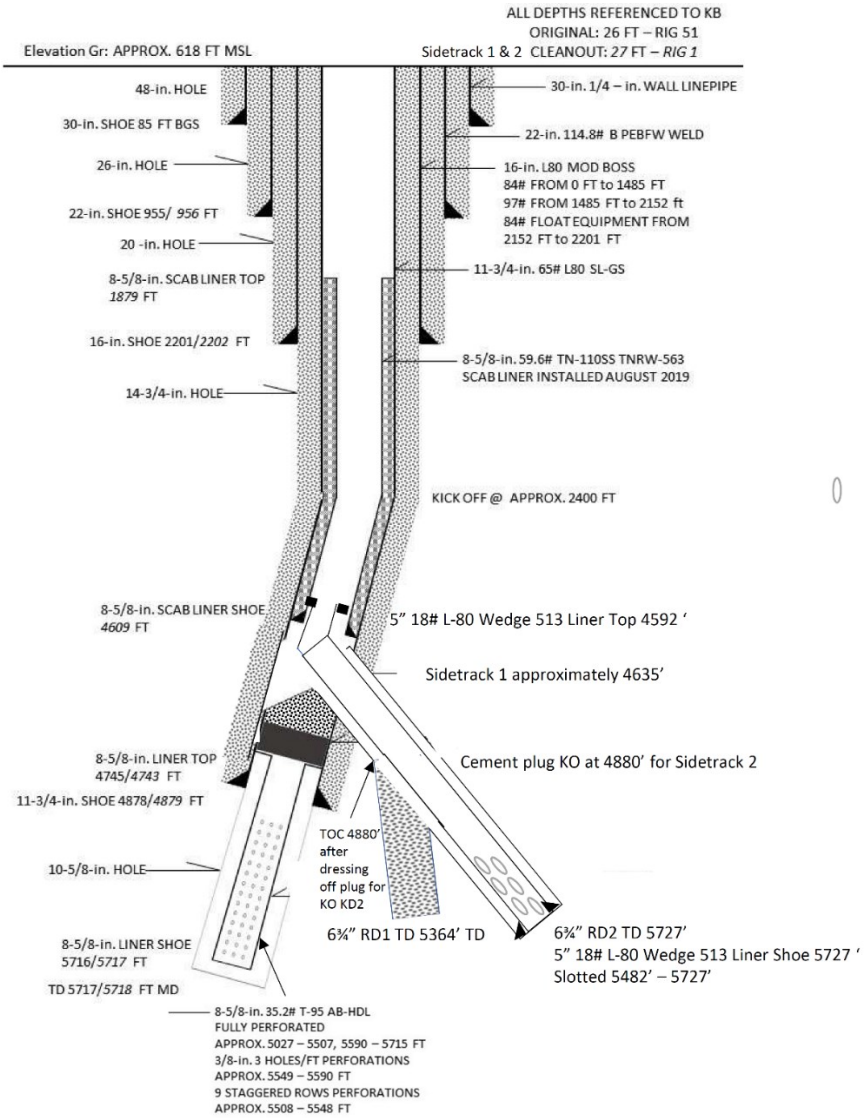

Figure 1: KS-14RD2 Well Design and Construction

2.2 Chemistry and Scaling in Seawater-Influenced Systems

KS-14 was routinely sampled following the start of production in 2021. Table 1 shows an average composition of the separated fluid and gas phases for approximately the first year of production (Q2 2021-Q1 2022). Brine and gas samples from production wells are collected in conjunction with the tracer flow test's (TFTs) conducted by Thermochem®. During this time, produced fluids from KS-14 were classified as Na-Cl type waters with moderate TDS (15,000 ppm) and field pH values of roughly 4.2-5.6, representing a variably mixed, thermally altered meteoric-modified seawater brine with up to roughly 40% seawater component. Some of the notable characteristics of the geothermal fluids compared to that of a typical seawater include depletion of sulfate, magnesium, sodium, and enrichment of silica and potassium, all of which are dominantly controlled by temperature dependent equilibrium reactions between the geothermal fluids and basalt host rock reservoir. Many of the trace elements are below or near analytical detection limits including zinc, lead, and copper. Iron concentrations have shown significant variation, especially immediately following plant startup. Anomalous values have been excluded in the average, as iron is impacted by sampling effects such as flow rate, filtering techniques, and sample preservation. As a result, reported dissolved iron concentrations contain great uncertainty, which may not be an accurate representation. Gas analyses show that the gas phase in the total discharge is less than 0.5 wt.% and is dominated by CO_2 and H_2S, with lesser amounts of H_2, N_2, CH_4, Ar and NH_3.

Sulfide scaling is a significant issue in geothermal systems with a seawater endmember fluid, as observed in the well-studied Reykjanes geothermal system in Iceland (Grant et al., 2020). Low solubility metal sulfides such as pyrite, galena, or sphalerite can precipitate due to decreasing temperature, increasing pH, and loss of dissolved H_2S during boiling in the near well aquifer or wellbore. For example, in Puna, sulfide scaling has been observed in production wells, separators, and within power station equipment (e.g., heat exchangers). The extent to which this scaling is due to residual metals from deep reservoir fluids or increased corrosion in the high-salinity Puna brines in combination with additional pH modification for silica management remains unclear. However, at Reykjanes, metal concentrations in downhole samples are significantly higher than at the surface. Hardardóttir et al. (2010) reported that at the surface, Reykjanes well RN19 had metal concentrations near detection limits (e.g., Fe 0.05 mg/kg, Zn 0.02 mg/kg, Cu 0.0008 mg/kg, Mn 1 mg/kg), compared to much higher concentrations in downhole samples (e.g., Fe 58 mg/kg, Zn 15 mg/kg, Cu 15 mg/kg, Mn 3 mg/kg). This suggests that metals precipitate before reaching the surface, correlating with sulfide deposition due to boiling in the well or near-wellbore. Thorolfsson (2019) noted that scaling at Reykjanes is mitigated by ensuring boiling occurs within the wellbore and therefore can be mechanically removed. In high-enthalpy fields such as Reykjanes (Iceland), Bouillante (Guadeloupe), and Svartsengi (Iceland), operational controls can limit flashing to within the wellbore due to the permeability, temperature and/or pressure conditions within the reservoir. At Puna however, some wells are unable to limit flashing to within the wellbore due to a lack of some of these reservoir conditions. Therefore, flashing can ultimately begin within the formation, contributing to permeability decline as a result of scaling within the formation. The scale-related decline in near-wellbore permeability and consequent increase in aquifer boiling results in productive feed zones transitioning from liquid saturated, to two-phase, and in some cases to single-phase steam. This drying out has been observed historically in several Puna wells.

Table 1: Average Phase Separated KS-14 Composition (Q1 2021-Q2 2022)

Separated Liquid Constituent	Concentration (mg/kg)	Separated Gas Constituent	Concentration (mmol/100molH_2O)
Cl	8,521	CO_2	67.3
SO4	11.0	H_2S	49.9
HCO_3	<2.7	H_2	9.9
Na	4,803	N_2	2.8
K	1,009	CH_4	0.23
Ca	115.4	Ar	0.06
Mg	0.21	NH_3	<0.01
SiO_2	937.5	Collection Conditions	
Fe*	0.14	Pressure (barg)	15.1
Mn	0.44	Enthalpy (kJ/kg)	2025
Zn	<0.02	*Average Fe concentrations excludes anomalous values (see text)	
Cu	<0.02		
Pb	<0.001		
pH (field/lab)	5.2/4.3		

3. RESULTS

3.1 Sample Collection and Analytical Methods

During the 2024 KS-14 workover program, a total of 14 solid debris samples were collected from depths ranging between 1,879 ft and 5,255 ft. Samples were collected using two techniques: boot basket/bottom hole assembly (BHA) collection and grab samples from the shaker deck. A sample matrix showing depth, collection method, wellbore liner location, and dominant mineralogy is provided in Table 2. Due to the sample collection methods utilized in this study, uncertainties exist with respect to quality and accuracy of sample data. Specifically, sample depths of boot basket/BHA samples inherently have a large margin of error. The use of a boot basket on the BHA assumes that the maximum depth reached by the tool corresponds to the depth in which the sample was collected. As a result, depths could be inaccurate as solid material could fall into the tool or stick to the BHA during insertion or removal of tool from the wellbore. While grab samples from the shaker deck are considered more reliable, uncertainty remains with respect to the depth in which the sample was collected. At depths of several thousand feet, a lag between the bit location and the sample material reaching the shaker deck is present. Samples collected at the shaker deck were assigned the same depth in which the bit was currently drilling.

All samples were submitted for whole-rock/clay fraction x-ray diffraction (XRD) and x-ray fluorescence (XRF). Upon logging of the samples, many samples contained what appeared to be drilling related and/or man-made material. Therefore, each sample underwent standard cleaning procedures including washing in soap and water, followed by drying in a low-temperature oven at 55°C.

Table 2: Sample Information

Depth (ft.)	Collection Method	Wellbore Location	Dominant Mineralogy
1,879	Shaker Deck	8-5/8” Scab Liner	Oxides (corrosion products)
3,007	Shaker Deck		Oxides (corrosion products)
3,636	Shaker Deck		Formation minerals
4,271	Shaker Deck		Carbonates/sulfates
4,592	BHA/Boot Basket	5” Slotted Liner	Oxides (corrosion products)
4,794	Shaker Deck		Oxides (corrosion products)
4,844	Shaker Deck		Oxides (corrosion products)
4,910	Shaker Deck		Formation minerals
4,954	Shaker Deck		Formation minerals
4,979	BHA/Boot Basket		Oxides (corrosion products)
4,980	Shaker Deck		Formation minerals
5,077	Shaker Deck		Formation minerals
5,081	BHA/Boot Basket		Formation minerals
5,255	BHA/Boot Basket		Formation minerals

3.2 XRD Mineralogy

Much of the recovered materials from KS-14 are consistent with the expected mineralogy of hydrothermally altered basalt host rock. These minerals consist of quartz, plagioclase feldspar, potassium feldspar, various clay minerals, clinopyroxene, and amphibole. Figure 2 displays the distribution of these minerals throughout the wellbore. These formation minerals are much more prominent in the lower section of the 5” liner, which is a directionally drilled portion of the well. At depths of 4,844 ft and greater, formation minerals are generally the dominant type of solid material, averaging roughly 60 wt.%, and up to 90 wt.% at the greatest depths. Within the shallower portions of the 5” liner and the entire 8-5/8” liner, formation mineral abundance drastically decreases to an average of less than 10 wt.%, excluding a single sample at 3,636 ft which shows elevated abundances formation minerals (~31 wt.%).

Mineralogical results also show that various oxides/oxyhydroxides are prominent throughout the wellbore. This group of minerals consists of goethite, hematite, magnetite, lepidocrocite, and ilmenite. Magnetite and goethite are both present throughout most of the depth profile, correlate to one another with depth, and are generally the most abundant oxides, as shown in Figure 3. They are prominent in the upper

portion of the 8-5/8" liner at depths of 1,879 ft to 3,007 ft (roughly 34-38 wt.%), as well as in the upper portion of the 5" liner at depths of 4,592 ft to 4,844 ft (roughly 20-37 wt.%). At greater depths, oxide/oxyhydroxide minerals generally decrease to less than 10 wt.%, with the exception of a single sample at 4,979 ft. However, the sample collected at 4,979' contained mostly metal fragments from the boot basket and may not be reflective of the material at that depth. A distinct change in mineralogy was noted in the area of the 5" liner top and in the 8-5/8" liner just above, which is a zone of the wellbore expected to host significant pressure drop during production due to the change in diameter. At this location hematite appeared as the most abundant oxide mineral (33 wt.%). Hematite was rarely detected at shallower depths and was present only at low concentrations (<5 wt.%) at greater depths. Lepidocrocite was generally detected at low concentrations (<5 wt.%) and showed a correlation to goethite and hematite, while ilmenite was only in the four deepest samples, but at low concentrations (<2 wt.%).

Carbonate and sulfate were found throughout the entire wellbore. These minerals include calcite, anhydrite and barite. This group of minerals represents a relatively small proportion of overall recovered material. In general, carbonates and sulfates range from 1-20 wt.%, averaging roughly 7 wt.% (excluding a single sample at a depth of 4,271 ft) and do not show a clear trend with respect to depth. The sample collected at 4,271 ft from the 8-5/8" liner above the 5" liner top shows uniquely elevated concentrations of these minerals at roughly 49 wt.%. Specifically, calcite and anhydrite are observed at concentrations of 17.5 and 30.2 wt. %, respectively. Siderite generally shows less than 1 wt.% throughout the entire depth profile, while concentrations of barite are generally below 2 wt.% throughout the depth profile but shows a peak of around 12 wt.% at the deepest sample depth.

Sulfide minerals including pyrite, sphalerite, and pyrrhotite were also detected throughout much of the sampled depth profile, as shown in Figure 4. Although observed in low concentrations, typically less than 10 wt.%, most of the sulfide minerals appear to be concentrated towards the intermediate depths, ranging between 3,636 ft to 4,979 ft. At depths less than, or greater than this range, sulfide concentrations average around 1.5 wt.%. Pyrrhotite is generally the most abundant sulfide mineral with concentrations of up to 10.8 wt.% at a depth of 3,636 ft. Unlike pyrrhotite, pyrite is not present in all samples. Rather, pyrite is more prominent in the deepest samples ranging from 4,980 ft to 5,255 ft and from 3,636 ft to 4,592 ft. In contrast, sphalerite is more prominent from 4,271 ft to 4,980 ft and absent in the shallowest and deepest sections of the wellbore.

Due to the XRD analytical method's reliance on crystal structure to determine mineralogy, significant proportions of the material were unable to be characterized due to the amorphous nature of the material. Elevated proportions of amorphous material were observed in samples collected from depths 1,879 ft to 4,979 ft. While the abundance of some of the amorphous component may rely on baseline corrections from the XRD data, it is likely that some amounts of amorphous material was collected from the wellbore. Other minerals detected at low concentrations, and not categorized in the above groups include siderite, xonotlite, and srebrodolskite.

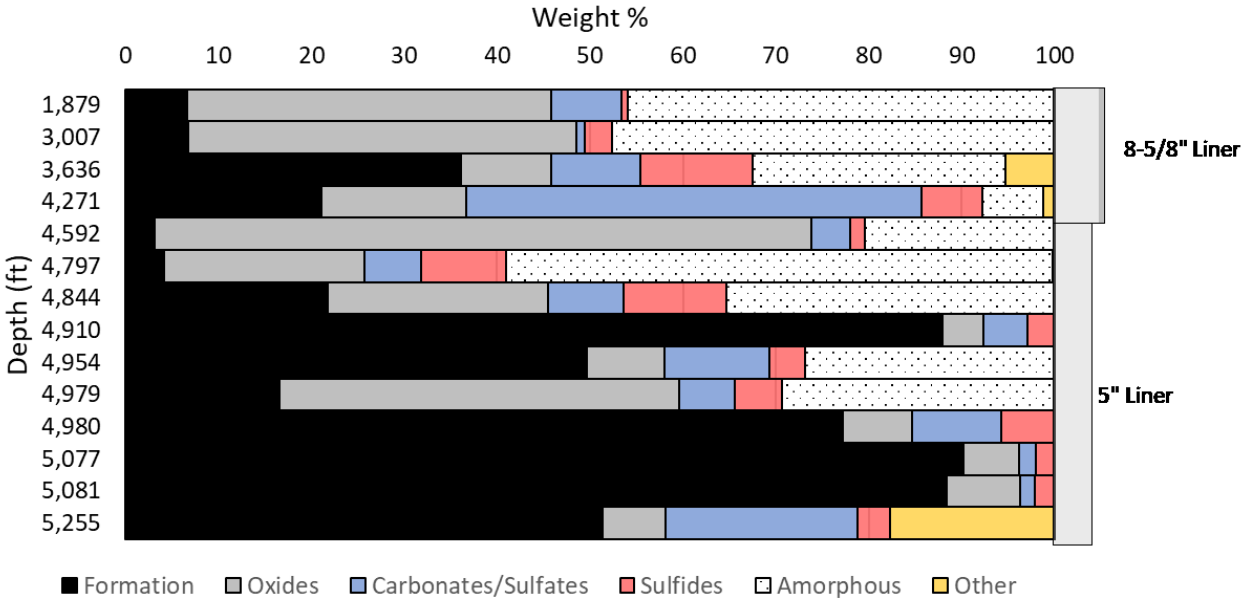

Figure 2: XRD General Mineralogic Distribution.

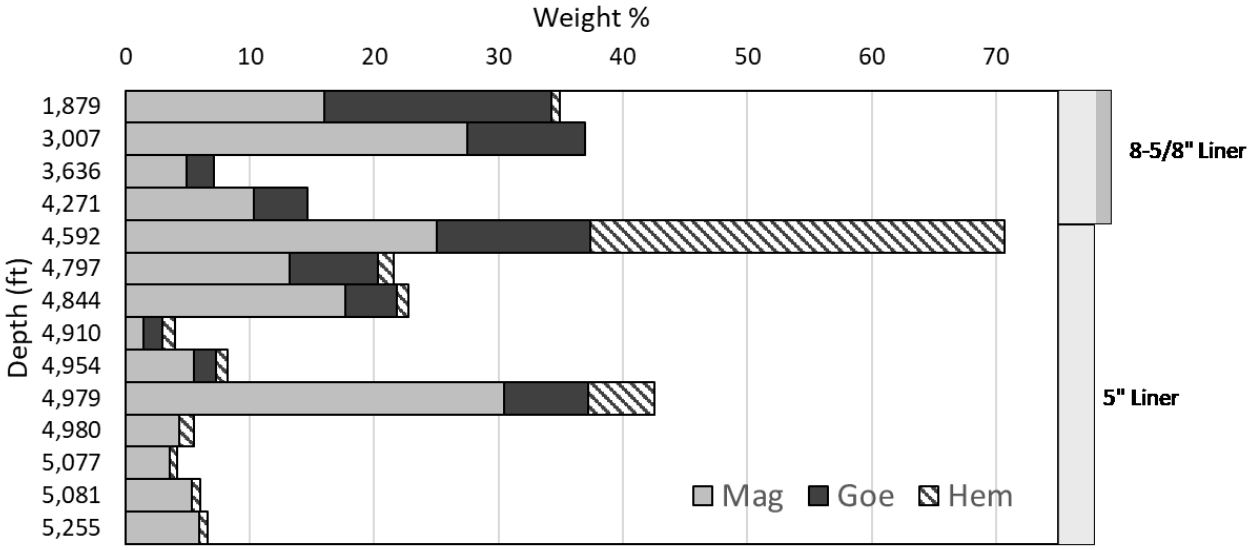

Figure 3: Distribution of magnetite (Mag), goethite (Goe), and hematite (Hem)

Figure 4: Distribution of sphalerite (Sph), pyrite (Pyr), and pyrrhotite (Pyrr)

3.3 XRF Elemental Composition

In general, iron is the dominant element throughout much of the depth profile and correlates with the abundance of oxides/oxyhydroxides observed in the XRD results (Figure 5). Specifically, elevated iron concentrations are observed in the upper portion of the 8-5/8" liner (1,879'-3,007'; ~19 wt.%) and 5" liner (4,592-4,844 ft and 4,979 ft, 16-21 wt.% and 19 wt.%). However, the sample from 4,979 ft was collected from the boot basket and contained large metal fragments. Therefore, it may not represent the true material at this depth. Other intervals generally contain less than 10 wt.% iron. Silicon is typically the next most abundant element. In general, intervals with dominant iron show low concentrations of silicon. The deeper portions of the depth profile generally have the greatest portion of silicon, with depths 4,910-5,255 ft (exception of 4,979 ft) showing greater than 6 wt.% silicon. An isolated shallower sample (3,636 ft) also shows elevated

concentrations of silicon at 14.4 wt.%, corresponding to the shallow depth containing abundant formation material. All other samples show less than 3.5 wt.% silicon. Depths that show the greatest amount of sulfur are generally deeper within the wellbore at depths ranging between 4,271-4,980 ft at concentrations of averaging roughly 4.5 wt.% and up to 9 wt.%. These abundances generally correlate with the abundance of metal sulfide minerals. Depths outside of this range generally contain less than 2 wt.% sulfur. Concentrations of calcium are generally greater in the deeper portions of the wellbore, below 4,844 ft, with an average concentration of 6 wt.%. The highest concentration of calcium (17.4 wt.%), however, is observed at a depth of 4,271 ft, correlating with the elevated concentration of carbonates/sulfates observed in XRD. Aluminum of 0.8 wt.% or greater are limited to the deeper portions of the wellbore, at depths of 4,844' or more. All shallower samples contain less than 1 wt.% aluminum. All other major elements are generally at lower concentrations (<1 wt.%) and more well distributed throughout the wellbore.

Three general trends are present in the trace element composition: 1) elements that are at similarly low concentrations at shallower depths, but increase in the deeper portions of the wellbore, 2) elements that show peak concentrations at middle to deeper portions of the depth profile, and 3) elements that show very low to below detection limit to be reliably measured throughout the entire depth profile (Figure 6). 1) Chromium, yttrium, zirconium, selenium, and niobium, generally have consistent concentrations throughout the wellbore that begin to increase at depths greater than 3,636 ft. The concentrations of these elements are typically below 100 ppm at the shallower depths and increase up to roughly 450 ppm, with the exception of niobium which remains below 25ppm. 2) Nickel, strontium, molybdenum, thorium, uranium, barium, zinc, and arsenic tend to show peak concentrations at depths ranging between 4,271 ft to 4,980 ft. Zinc is generally the greatest trace element of all elements analyzed by two orders of magnitude. Strontium, thorium, uranium, molybdenum, and nickel show peak concentrations at depths ranging between 4,592 ft and 4,794 ft at concentrations generally above 2,000 ppm and decrease significantly at greater depths. In addition, a single barium concentration of roughly 90,000 ppm at 5,255 ft likely represents laboratory error. 3) Copper, cobalt, rubidium, lead, and gallium generally show very low, to below detection limit concentrations. Occasional peaks of concentrations are present, but generally below 200 ppm.

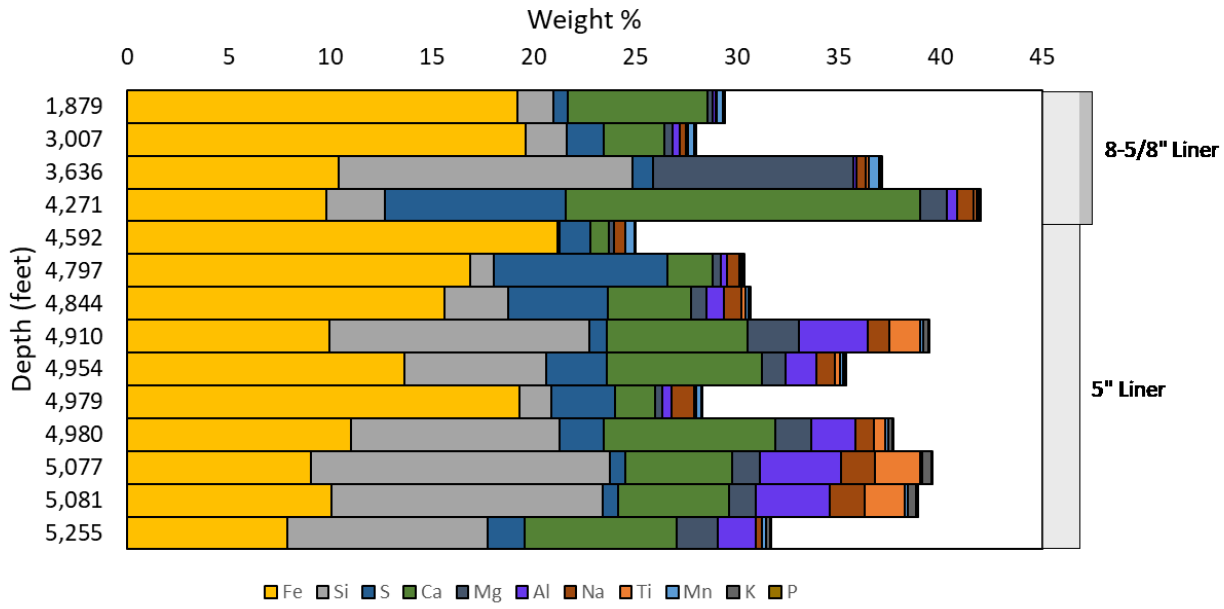

Figure 5: XRF Major Elemental Composition

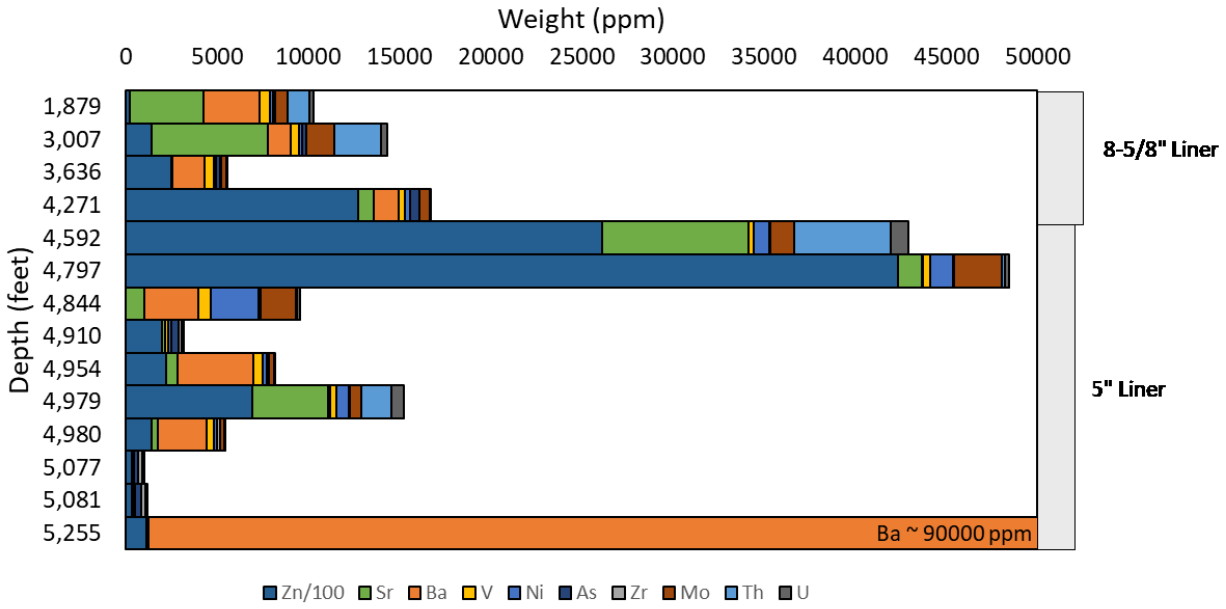

Figure 6: XRF Trace Element Composition

4. DISCUSSION

4.1 Formation Material Migration

Some of the recovered material during the KS-14 workover program can be attributed to formation materials that have accumulated in the directionally drilled 5" slotted liner. Specifically, crystalline formation minerals including quartz, plagioclase feldspar, potassium feldspar, clinopyroxene, amphibole, and various clay minerals are dominant at depths of 4,844 ft and greater. These results suggest that much of the material collected within this portion of the wellbore migrated through the slotted liner. Since the 5" liner is sub-vertical, material was able collect along the liner interior, rather than falling to the bottom of the wellbore. Limited formation material is found in the upper portion of the 5" liner, and any portion of the vertical 8-5/8" liner.

All samples in this study were collected above the slotted portion of the liner, which is located at a depth interval of 5,482-5,727 ft. Therefore, formation material was able to accumulate up to roughly 500 linear ft within the wellbore, potentially capable of impacting well productivity. In fact, all active production wells at PGV contain rock catchers at the wellhead, designed to capture any solids material at surface. PGV personnel have observed accumulation of solid material within these rock catcher units. Therefore, it is well documented that formation material migrates from depth to the surface. It is assumed that much of the formation material migrated into the wellbore during two-phase production at KS-14, rather than during single-phase steam production. This assumption is based on the fact that during two-phase production, flow velocities tend to be greater, and the brine phase has the viscosity capable of carrying formation material within the flowing stream.

4.2 Paleo Flash Depth and Sulfide Scale

One of the most notable mineralogical changes observed is the presence of a high proportion of calcite and anhydrite corresponding to a depth of 4,271 ft. While these minerals have been observed to a limited extent in the cuttings of various wells at PGV, they are typically noted in trace concentrations and are not commonly associated with PGV reservoir brines due to the relatively low pH and elevated temperatures of the reservoir fluids. In addition, scale minerals collected within surface equipment are mainly dominated by amorphous silica. Therefore, the presence of abundant calcite and anhydrite at-depth likely represents influence from an external mechanism, such as significant flashing within the wellbore. Since KS-14 was producing from a two-phase feed zone immediately following start-up (1/25/2021), a brine phase was present within the wellbore. The location in which calcite and anhydrite was observed may represent a paleo flash depth, corresponding to a depth in which significant phase separation had been occurring. The sample depth of 4,271 ft is the sample located closest to the change in liner diameter. The change in wellbore geometry at this location could drive a localized pressure drop, driving additional flashing, decreasing brine fraction, increasing constituent concentration, and subsequent precipitation of calcite and anhydrite. As KS-14 continued to produce, the brine level continued to drop until flashing had extended into only the formation and single-phase steam production dominated until the failure of the well.

Sulfide minerals are also present throughout much of the depth profile and may be related to scaling mechanisms such as adiabatic boiling and associated pH changes. These sulfide minerals consist of mainly pyrrhotite, sphalerite and pyrite (Figure 4). While some sulfide minerals, such as pyrite, are present within natural geothermal systems (Simmons and Browne, 2000; Stone and Fan, 1978), much of the sulfide minerals are interpreted to be a result of wellbore scaling. Numerous studies have shown that geothermal systems, including many seawater-influenced systems have produced these types of metal-sulfide scale in both single and two-phase wells (Hardardóttir et al.,

2013; Karabelas et al., 1989; Thorolfsson, 2019). Analogous seawater-influenced geothermal systems such as Reykjanes have observed metal sulfide scale interpreted to be driven mainly by a decrease in pressure within the wellbore (Hardardottir et al., 2005). A series of field studies showed that the order in which metal sulfides precipitated with decreasing pressure was wurtzite/sphalerite (ZnS), galena (PbS), chalcopyrite ($CuFeS_2$), bornite (Cu_5FeS_4), followed by amorphous silica at lowest pressure. The distinct interval of sphalerite (3,636-4,980ft) observed in KS-14 may therefore indicate the region within the wellbore in which sulfides were precipitating at highest pressure. One of the primary mechanisms that could cause these scaling events is wellbore flashing leading to loss of CO_2 and H_2S from the liquid phase and decreasing temperature, subsequently reducing the solubility of sulfide minerals and destabilization of chloride-metal complexes. H_2S loss would further favor the precipitation of metals transported by sulfide complexes (Harðardóttir et al. 2001, Harðardóttir, 2002). Furthermore, wellbore flashing would subsequently increase the concentration of these dissolved metals in the brine phase, likely until saturated conditions have been reached. The presence of pyrite may indicate formation mineralogy at the deepest intervals of the well but may represent secondary scale precipitation in conjunction with other metal sulfides as pressure continued to drop and the well transitioned to single-phase steam. Pyrrhotite has been observed as both a sulfide scale and a corrosion product (Hardardóttira et al., 2013, Ward et al., 2006). Therefore, the mechanism proposed to cause formation of pyrrhotite is unclear, yet it's correlation with other metal-sulfides and lack of correlation with other interpreted corrosion products such iron-oxides suggest that it precipitates within the wellbore as a secondary sulfide scale.

4.3 Corrosion

Iron-rich solid material interpreted to be related to corrosion mechanisms have been observed within surface equipment and piping at PGV historically. However, prior to this study, limited downhole samples had been collected showing significant proportions of iron-rich material. Numerous metal-oxides/oxyhydroxides were observed throughout the entire sampled wellbore (Figure 3). The greatest of abundance of these minerals were observed near the junction of the 8-5/8" liner and the 5" liner (4,592 ft), as well as shallow depths of less roughly 3,000 ft. In nearly all sampled material, magnetite dominates the proportion of these oxide minerals, while hematite is often well below 5 wt.%. However, at the junction between 8-5/8" liner and the 5" liner, hematite abundance significantly increases to roughly 33 wt.%, becoming the most dominant iron-bearing mineral. The high abundance of hematite relative to other iron-oxide minerals at this depth is unique in that the redox environment is generally believed to be reducing within geothermal brines, limiting the available oxygen for the precipitation of hematite. The mechanisms behind precipitation of hematite in this context is not well understood and needs further evaluation. In the deeper portions of the well (4,844 ft and deeper), where formation minerals dominate, the relatively low abundance of magnetite and hematite are likely representative of the hydrothermally altered basalt host rock. However, above this depth, abundance of hematite, magnetite, and goethite dominate the proportion of material collected. While this could represent a lack of formation material at these depths, the increase in proportion as well as a change in relative amounts of hematite, goethite, and magnetite compared to the deep samples could suggest that corrosion is more pronounced above 4,910 ft. Lastly, the changes in the geochemical signature of the Puna reservoir fluids following the eruption likely impacted the corrosive nature of the reservoir fluids. Therefore, the extent of corrosion within KS-14 is difficult to determine and likely does not reflect historic or future characteristics as the reservoir chemistry transitions to near pre-eruption conditions.

5. CONCLUSION

KS-14 was successfully brought online following the 2018 Kilauea eruption as a redrill of the original production hole. During a period of transient geochemical conditions and after two and a half years of production, the well transitioned from two-phase flow to single-phase steam production. Shortly thereafter, the well stopped flowing entirely. A workover program was implemented in which a number of solid samples were recovered from a variety of depths ranging from 1,879-5,255 ft. Mineralogical and elemental analysis provided insight to the types of scale found throughout the wellbore.

Within much of the 5" liner, formation material consisting of quartz, plagioclase feldspar, potassium feldspar, clinopyroxene, amphibole, and various clay minerals are dominant. These results suggests that a significant proportion of formation material migrated through the slotted portion of the liner and accumulated several hundred feet within the sub-vertical section of the well. A dominant interval of calcite and anhydrite is located immediately above the junction between the 5" liner and the 8-5/8" liner. The presence of these minerals suggest that significant flashing likely occurred around this depth, potentially driven by the change in liner geometry and subsequent localized decrease in pressure. Sulfide minerals were found throughout the sampled depth interval and consist of sphalerite, pyrite, and pyrrhotite. While minor amounts of pyrite and pyrrhotite are present within the formation minerals, the onset of sphalerite precipitation likely represents the first instance of sulfide scale from the brine as pressure began to decrease. Additional pyrrhotite and pyrite may also contribute to secondary precipitation as pressure continued to decrease within the wellbore. Lastly, corrosion related materials are reflected in the high abundances of iron-oxide/oxyhydroxide minerals. The dynamic reservoir geochemical conditions immediately following the eruption may have contributed to the scale types observed in this study but may not reflect the expected scale types as the reservoir returns to near pre-eruption conditions.

ACKNOWLEDGEMENTS

The authors thank Ormat Technologies, Inc. for permission to publish this work. In addition, the authors would like to thank the work of the PGV operations team and rig operations team for safely implementing the KS-14 workover program and collecting all samples on-site.

REFERENCES

Anderson, A.T., Wright, T.L., (1972). "Phenocrysts and Glass Inclusions and Their Bearing on Oxidation and Mixing of Basaltic Magmas, Kilauea Volcano, Hawaii." American Mineralogist, Vol. 57, pp. 188-216.

Gerlach, T.M. (1993). "Oxygen buffering of Kilauea volcanic gases and the oxygen fugacity of Kilauea basalt." Geochemica et Cosmochimica Acta, Vol. 57, pp. 793-814

Grant, H., Hannington, M.D., Hardardóttir, V., Fuchsa, S.H., Schumannd, D. 2020. Trace metal distributions in sulfide scales of the seawater-dominated Reykjanes geothermal system: Constraints on sub-seafloor hydrothermal mineralizing processes and metal fluxes. Ore Geology Reviews 116 (2020) 103145.

Hardardóttir, V., Kristmannsdóttir, H. and Ármannsson, H.: Scale Formation in Wells RN-9 and RN-8 in the Reykjanes Geothermal Field, Iceland, Water-Rock Interaction, (2001), ISBN90 2651 824 2, 851-854

Hardardóttir, V.: Scales in Well 9 Reykjanes, Report OS-2002/011, (2002)

Hardardóttir, V., Thorhallsson, S., and Ármannsson, H.: Characterization of Sulfide-Rich Scales in Brine at Reykjanes, Proceedings, World Geothermal Congress, (2005).

Hardardóttir, V., Hedenquist, J.W., Hannington, M.D., Brown, K., Fridriksson, TH., and Thorhallsson, S. 2010. Composition of Reservoir Liquid and Metals in Pipeline Scale, Reykjanes Geothermal System, SW Iceland. Proceedings World Geothermal Congress 2010.

Hardardóttir, V, Hannington, M., and Hedenquist, J.: Metal Concentrations and Metal Deposition in Deep Geothermal Wells at Reykjanes High-Temperature Area, Iceland, Procedia Earth and Planetary Sciences 7, (2013), 338-341.

Karabelas, A.J., Andritsos, N., Mouza, A., Mitrakas, M., Vrouzi, F., Christanis, K.: Characteristics of Scales from the Milos Geothermal Plant, Geothermics, vol. 18, (1989). 169-174

Murphy, J., Prina, N., Spielman, P., Spake, D.: Permeability and Numerical Modeling of the Puna Geothermal Venture, GRC Transactions, vol. 48, (2024).

Simmons, S.F. and Browne, P.L.: Hydrothermal Minerals and Precious Metals in the Broadlands-Ohaaki Geothermal System: Implications for Understanding Low-Sulfidation Epithermal Environments, Economic Geology, vol 95, (2000), 971-999

Spake, D., Reynolds, Z., Caro, D., Prina, N., Murphy, J., Johnson, A., Spielman, P., Zuza, R., and Webbison, S.; Conceptual Model of the Puna Geothermal System, GRC Transactions, vol. 48, (2024).

Spielman, P., Drakos, P., Tennison, J., Prina, N., Bakane, P., and Dahl, G.: Damage and Repair of Puna Well KS-14. GRC Transactions, vol. 44, (2020).

Stone, A., and Fan, P.: Hydrothermal Alteration of Basalts from Hawaii Geothermal Project Well-A, Kilauea, Hawaii, Geology, vol. 6, (1978), 401-404.

Thorolfsson, G. 2019. Scaling problems in HS Orka's Geothermal Power plants, an overview; Conference: CORROSION 2019.

Ward, K.T., Brown, K.L., Wester-Brown, J.: Mineral Precipitation in the Rotokawa Geothermal Power Station, New Zealand, Proceedings, 28th NZ Geothermal Workshop, (2006).